Astron. Astrophys. 334, 703–712 (1998)

ASTRONOMY AND ASTROPHYSICS

Helioseismic constraints on new solar models from the MoSEC code

J.R. Elliott

JILA, University of Colorado, Boulder, CO 80309-0440, USA

Received 11 September 1997 / Accepted 24 February 1998

Abstract. Evolutionary solar models are computed using a new stellar evolution code, MoSEC (Modular Stellar Evolution Code). This code has been designed with carefully controlled truncation errors in order to achieve a precision which reflects the increasingly accurate determination of solar interior structure by helioseismology. A series of models is constructed to investigate the effects of the choice of equation of state (OPAL or MHD-E, the latter being a version of the MHD equation of state recalculated by the author), the inclusion of helium and heavy-element settling and diffusion, and the inclusion of a simple model of mixing associated with the solar tachocline. The neutrino flux predictions are discussed, while the sound speed of the computed models is compared to that of the sun via the latest inversion of SOI-MDI p-mode frequency data. The comparison between models calculated with the OPAL and MHD-E equations of state is particularly interesting because the MHD-E equation of state includes relativistic effects for the electrons, whereas neither MHD nor OPAL do. This has a significant effect on the sound speed of the computed model, worsening the agreement with the solar sound speed. Using the OPAL equation of state and including the settling and diffusion of helium and heavy elements produces agreement in sound speed with the helioseismic results to within about $\pm 0.2\%$; the inclusion of mixing slightly improves the agreement.

Key words: Sun: evolution – Sun: interior – Sun: oscillations

1. Introduction

Most of the differences between observed p-mode frequencies and those calculated from evolutionary solar models are believed to reflect uncertainties in the ingredients of solar modelling. Much effort has consequently been applied to finding which aspects of the uncertain physical assumptions are responsible for the differences between observation and theory (e.g. Turck-Chièze & Lopes 1993). This has led, for example, to the use of the MHD equation of state (Mihalas et al. 1988), the improved calculation of opacity in the OPAL tables (Iglesias & Rogers 1991; Rogers & Iglesias 1992), the inclusion of the effects of helium settling and diffusion (Bahcall & Pinsonneault 1992b; Christensen-Dalsgaard et al. 1993), and finally the development of models with heavy element settling and diffusion (Proffitt 1994; Bahcall & Pinsonneault 1995).

Several components go into a typical recipe for solar evolution: these include a set of opacity tables, a set of equation of state tables, and a set of reaction rates and temperature dependences for each appropriate nuclear reaction. Additional assumptions concern the choice of convection theory used, the model of the solar atmosphere employed, and various input parameters, such as present-day solar age and luminosity. Given a certain set of choices for each of these ingredients, any evolution calculation should ideally give the same result to within the numerical accuracy of its integration scheme. Much progress has been made towards attaining this goal (e.g. Christensen-Dalsgaard 1991a) by eliminating the errors in complex evolution codes which previously caused them to disagree.

Given the accuracy with which p-mode frequencies are currently being measured by such instruments as SOI-MDI (Kosovichev et al. 1997) and GONG (Harvey et al. 1996), subtle aspects of the input physics are becoming subject to scrutiny. In order to facilitate such progress, not only should errors be eliminated in evolution codes, but also codes should be developed with very carefully controlled truncation errors, such as the CESAM code described by Berthomieu et al. (1993). With these considerations in mind, we have developed a new stellar evolution package named MoSEC, designed with minimization and control of truncation errors very much to the fore.

MoSEC is used to generate a series of seven evolutionary solar models with varying input physics. These are designed to investigate the effect of including settling and diffusion of helium and heavy elements, the effect of the choice of equation of state, the effect of ignoring the variation of the heavy-element abundance in the calculation of the equation of state (as has been done by various authors), and the effect of mixing below the base of the convection zone. The neutrino flux predictions are compared to measured solar values, while the sound-speed is compared to that of the sun using an inversion of the latest SOI-MDI p-mode frequencies. In the case of the equation of state, MHD-E is a new MHD-like calculation taking into account the relativistic correction to the electron pressure, a correction which was not included in either the OPAL or the

Send offprint requests to: J.R. Elliott

original MHD equations of state. A solar model is calculated using MHD-E equation of state, and compared to two models, one calculated with OPAL, and the other also calculated with OPAL, but adding in the relativistic correction to the electron pressure. The last model enables us to evaluate what fraction of the difference between the OPAL and MHD-E models arises from the different treatment of the electron pressure.

2. Formulation of the problem

2.1. General principles

The term "standard solar model" defines a certain set of simplifying assumptions under which the calculation of stellar evolution may more easily be performed. A uniform initial chemical composition is assumed, rotation, magnetic fields and mass loss are neglected, and spherically-symmetric hydrostatic equilibrium is imposed. Mass is chosen as the independent variable rather than radius, since the equations of stellar structure become less nonlinear.

The partial differential equations of stellar evolution are as usual expressed as two sets of ordinary differential equations: one that describes the equilibrium structure at a particular time given the chemical composition, and another that describes the evolution with time of the chemical composition. The solution of the former is discussed in Sect. 2.2, and the latter in Sect. 2.5.

2.2. Spatial integration

The equations describing the equilibrium structure of a solar model are fourth order, with two boundary conditions each at the centre and surface. These were originally solved by the shooting technique, whereby the equations were integrated inwards from the surface and outwards from the centre, the matching being achieved by varying the four free parameters (central pressure and temperature, surface radius and luminosity). This technique has largely been superceded by the Henyey relaxation method.

An N-point grid m_i ($i = 1, \ldots, N$ with $m_N = M_\odot$) is imposed, and the differential equations are replaced by a set of finite-difference equations. Originally these finite-difference equations were second order, but MoSEC uses a fourth-order scheme described by Cash & Moore (1980). $N-1$ further grid points $m_{3/2} \ldots m_{N-1/2}$ are interleaved midway between pairs of the original N grid points. Equations are then constructed for each of the dependent variables, pressure (p), temperature (T), luminosity (L) and radius (R); for example,

$$p_{i+1} - p_i = \frac{1}{6}(m_{i+1} - m_i)\left(p'_i + 4p'_{i+1/2} + p'_{i+1}\right) , \quad (1)$$

where $'$ denotes the derivative with respect to the independent variable, m. $p_{i+1/2}$ is given by

$$p_{i+1/2} = \frac{1}{2}(p_i + p_{i+1}) - \frac{1}{8}(p'_{i+1} - p'_i)(m_{i+1} - m_i) . \quad (2)$$

Similar equations are used for T, L and R. The derivatives on the right-hand sides of Eqs (1) and (2) are known functions of p, T, L and R through the equations of stellar structure.

This large system of equations is solved by a series of Newton-Raphson iterations until convergence has been obtained. This requires the knowledge of the partial derivatives of p', T', L' and R' with respect to p, T, L and R. Some of these derivatives may be evaluated analytically, but for others (such as those involving the equation of state or opacity tables) numerical derivatives have to be employed. Each iteration requires the solution of a linear system of equations, through the inversion of a block diagonal matrix. It is important in such a relaxation scheme to have initial conditions sufficiently close to the true solution; two Runge-Kutta integrations, one outward from the centre and one inward from the surface, are used to provide such an initial trial solution.

2.3. Boundary conditions

Boundary conditions are imposed at the centre and at the surface. At the centre,

$$L_1 = \frac{4\pi}{3}R_1^3\rho_1\varepsilon_1\left\{1 - \frac{1}{5}R_1^2\left[\left(\left.\frac{\partial \ln \varepsilon_{\rm eqb}}{\partial \ln p}\right|_T + 1\right)\frac{\partial^2 \ln p}{\partial r^2} + \left(\left.\frac{\partial \ln \varepsilon_{\rm eqb}}{\partial \ln T}\right|_p - 1\right)\frac{\partial^2 \ln T}{\partial r^2}\right]\right\} , \quad (3)$$

$$m_1 = \frac{4\pi}{3}R_1^3\rho_1\left[1 - \frac{1}{5}R_1^2\left(\frac{\partial^2 \ln p}{\partial r^2} - \frac{\partial^2 \ln T}{\partial r^2}\right)\right] , \quad (4)$$

where ε denotes the energy-generation rate per unit mass, and $\varepsilon_{\rm eqb}$ the equilibrium energy-generation rate at the centre. At the surface,

$$T_N = T(\tau_{\rm b}, T_{\rm eff}) , \quad (5)$$

$$p_N = p(\tau_{\rm b}, T_{\rm eff}) , \quad (6)$$

where $T_{\rm eff}$ is the effective temperature, given by $T_{\rm eff}^4 = L_N/4\pi\sigma R_N^2$ (σ is the Stefan-Boltzmann constant), and $\tau_{\rm b}$ is the optical depth at which interior solution is matched to the atmosphere. The latter should be made sufficiently large that the diffusion approximation (upon which the radiative-transfer equation is based) is valid (Morel et al. 1994). Assuming the HSRA $T(\tau, T_{\rm eff})$ law, as fitted by Ando & Osaki (1975),

$$T(\tau, T_{\rm eff}) = \tfrac{3}{4}T_{\rm eff}^4\left[\tau + 1.017 - 0.3\exp(-2.54\tau) - 0.291\exp(-30\tau)\right] , \quad (7)$$

$T(\tau_{\rm b}, T_{\rm eff})$ is obtained directly, and $p(\tau_{\rm b}, T_{\rm eff})$ is obtained by integrating for the structure of the atmosphere using a Runge-Kutta scheme with adaptive step size.

2.4. Truncation error

If h is the step size in mass, then the local truncation error in Eq. (1) is $O(h^5)$. This gives a global truncation error which scales like h^4, so the finite-difference scheme is fourth order. This is demonstrated in Fig. 1, which plots the logarithm of the

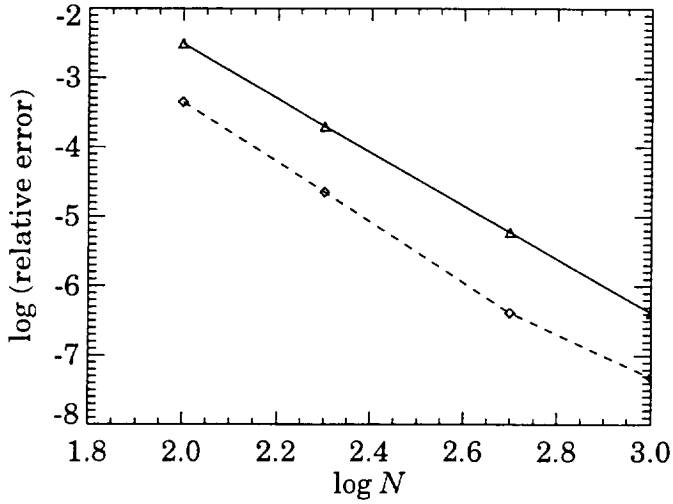

Fig. 1. Logarithm of the relative errors in radius (solid line) and luminosity (dashed line) plotted against the logarithm of the number of radial grid points, N.

relative errors in radius and luminosity against $\log N$. The slight departure of the errors in luminosity from following a straight line is probably due to errors arising from the interpolation of opacity and equation of state tables. A value of $N = 1000$ is sufficient to constrain the relative truncation errors in radius and luminosity to $\lesssim 10^{-6}$.

2.5. *Nuclear burning*

The treatment of the time evolution of chemical composition is crucial to the success of a stellar evolution code. The principal energy-generating cycle of the proton-proton chain (which dominates in the sun) consists of two halves, the conversion of hydrogen into ^{3}He via deuterium, and the fusion of ^{3}He to form ^{4}He. In the centre of the sun, the second of these reactions proceeds very much faster than the first, so that equilibrium of ^{3}He is quickly established. Away from the centre, equilibrium takes much longer to be reached, so it is essential to follow the evolution of the ^{3}He abundance correctly in order to calculate the total luminosity accurately. Since the time scales of the two reactions of the principal branch of the proton-proton chain are so different, the equations constitute a stiff system, and should be integrated by an appropriate implicit technique.

Christensen-Dalsgaard (1991a) used a backward Euler method for evolving the ^{3}He abundance, and a second-order scheme for the evolution of the hydrogen abundance. Subsequent codes have employed more sophisticated integration schemes; for instance, the CESAM code developed by Morel et al. (1990) uses an implicit, second-order, time-integration scheme. MoSEC uses a similar second-order implicit method for determining the time evolution of the abundances of H, ^{3}He, ^{4}He, ^{12}C, ^{13}C, ^{14}N, and ^{16}O. To simplify the reaction network, ^{7}Be is assumed to be always in equilibrium, while only the dominant branches are considered in the CNO cycle.

The reaction rate $r_p \equiv r_p(m_i, t)$, corresponding to process p (as defined in Table 1) at the point $m = m_i$, is then given by

Table 1. Simplified nuclear reaction network.

p	Reaction
1	^{1}H(p, $\beta^+\nu$)^{2}H(p, γ)^{3}He
2	^{3}He(^{3}He, 2p)^{4}He
3	^{3}He(α, γ)^{7}Be(β^-, ν)^{7}Li(p, α)^{4}He
4	^{12}C(p, γ)^{13}N(, $\nu\beta^+$)^{13}C
5	^{13}C(p, γ)^{14}N
6	^{14}N(p, γ)^{15}O(, $\nu\beta^+$)^{15}N(p, α)^{12}C
7	^{16}O(p, γ)^{17}F(, $\nu\beta^+$)^{17}O(p, α)^{14}N

one of the following equations (in units of $\mathrm{s}^{-1}\mathrm{g}^{-1}$):

$$r_1 = c_1 X_1 X_1 , \tag{8}$$
$$r_2 = c_2 X_3 X_3 , \tag{9}$$
$$r_3 = c_3 X_3 X_4 , \tag{10}$$
$$r_4 = c_4 X_1 X_{12} , \tag{11}$$
$$r_5 = c_5 X_1 X_{13} , \tag{12}$$
$$r_6 = c_6 X_1 X_{14} , \tag{13}$$
$$r_7 = c_7 X_1 X_{16} , \tag{14}$$

where $X_n \equiv X_n(m_i, t)$ is the fractional abundance by mass of the element with atomic number n, and $c_p \equiv c_p(m_i, t)$ is the reaction-rate coefficient for process p. The latter are functions of density and temperature alone. The evolution of the elemental abundances is then calculated according to the following set of equations:

$$\frac{\mathrm{d}X_1}{\mathrm{d}t} = a_1 (2r_2 - 3r_1 - r_3 - r_4 - r_5 - 2r_6 - 2r_7) , \tag{15}$$
$$\frac{\mathrm{d}X_3}{\mathrm{d}t} = a_3 (r_1 - 2r_2 - r_3) , \tag{16}$$
$$\frac{\mathrm{d}X_4}{\mathrm{d}t} = a_4 (r_2 + r_3 + r_6 + r_7) , \tag{17}$$
$$\frac{\mathrm{d}X_{12}}{\mathrm{d}t} = a_{12} (r_6 - r_4) , \tag{18}$$
$$\frac{\mathrm{d}X_{13}}{\mathrm{d}t} = a_{13} (r_4 - r_5) , \tag{19}$$
$$\frac{\mathrm{d}X_{14}}{\mathrm{d}t} = a_{14} (r_5 - r_6 + r_7) , \tag{20}$$
$$\frac{\mathrm{d}X_{16}}{\mathrm{d}t} = a_{16} (-r_7) . \tag{21}$$

where a_n is the atomic mass of the element with atomic number n.

2.6. *Diffusion and gravitational settling*

The relative abundances of chemical elements in the solar interior are modified not only by nuclear burning, but also by the motion of atoms of different species with respect to one another. Gravitational and radiative forces acting on individual atoms drive such motions, while interactions between atoms tend to redistribute momentum in a random way and thereby

counteract these forces. The details of element segregation in the sun are determined by the exact nature of the competition between these processes in a multi-component plasma.

Since the abundances of the heavy elements are small, it is a reasonable approximation to treat them as if they were trace elements in a H-He background (Proffitt 1994). The seven species discussed in the context of nuclear reactions (H, ^{3}He, ^{4}He, ^{12}C, ^{13}C, ^{14}N, and ^{16}O) are treated individually in the settling and diffusion calculation, and are assumed to be fully ionized, while all the other heavy elements are grouped together and assumed to diffuse like fully ionized iron. Since the diffusion of heavy elements has a relatively small effect on the properties of the computed model, this represents a good approximation (Bahcall & Pinsonneault 1995).

The simplified transport equations of Michaud & Proffitt (1993) are used to describe the gravitational settling and diffusion of helium and the heavy elements. The diffusion velocities given by these equations are accurate to within about 10% when compared to the more rigorous derivation of Burgers (1969). The equations are solved using an explicit, second-order, time integration scheme, with time steps determined by the overall truncation error requirement.

2.7. Time evolution

An Q-point grid in time, t_j, is constructed such that $t_1 = 0$ and $t_Q = t_\odot$, where $t_\odot$ is the age of the sun. In order to evolve the solar model from time t_j to time t_{j+1}, assuming the structure $p_{i,j} \equiv p(m_i, t_j)$, $\rho_{i,j} \equiv \rho(m_i, t_j)$, $T_{i,j} \equiv T(m_i, t_j)$ to be known at t_j, the following procedure is adopted:

1. The coefficients $c_{p;i,j} \equiv c_p(m_i, t_j)$ are evaluated using the known values of $\rho_{i,j}$ and $T_{i,j}$. The coefficients $c_{p;i,j+1}$ are initially assumed to be equal to $c_{p;i,j}$.
2. Eqs. (15)-(21) are integrated assuming the coefficients $c_p(m_i, t)$ take the values

$$c_p(m_i, t) = \frac{t - t_j}{t_{j+1} - t_j} c_{p;i,j+1} + \frac{t_{j+1} - t}{t_{j+1} - t_j} c_{p;i,j} \,. \qquad (22)$$

3. The structure is evaluated at time t_{j+1}, using the new hydrogen abundance so obtained. This yields a new set of values for $c_{p;i,j+1}$.
4. Steps 2 and 3 are repeated until satisfactory convergence has been obtained.

The grid points t_j are not distributed uniformly in time: in the early stages of evolution they are much more closely spaced than later on. The distribution is given by the functional form

$$\frac{t_j}{t_\odot} = \frac{\tanh(4x - 3) - \tanh(-3)}{\tanh(1) - \tanh(-3)} \,, \qquad (23)$$

where $x = (j - 1)/(Q - 1)$. The exact function chosen to define the grid in time does not affect the rate of convergence of the solution as Q is increased, but does affect the actual truncation error for a particular value of Q. The form (23) is chosen as it gives a particularly low truncation error. Since the procedure used to update the chemical composition between t_j and t_{j+1} is second-order, the truncation error in the final model at time $t_\odot$ goes like Q^{-2}. In order to exploit this known dependence, a series of increasing trial values of Q is used, and the final result is obtained by Richardson extrapolation. In order to demonstrate this, Fig. 2 shows how the truncation error in radius and luminosity varies with Q; the logarithm of the relative error in each of these quantities is plotted against $\log Q$ for $Q = 10, 20, 40, 80$. While the relative error is still larger than 10^{-5} for $Q = 80$, Richardson extrapolation enables the radius and luminosity to be estimated to an accuracy of better than 10^{-6} using just $Q = 10, 20, 40$.

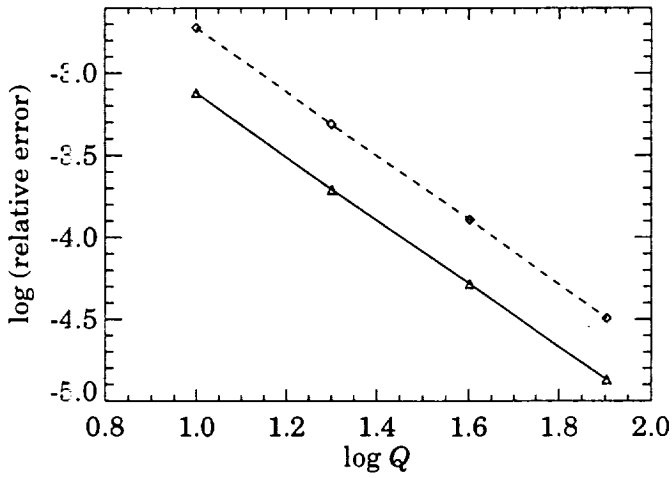

Fig. 2. Logarithm of the relative errors in radius (solid line) and luminosity (dashed line) plotted against the logarithm of the number of temporal grid points, Q.

2.8. Calibration of mixing length and initial hydrogen abundance

The final values at time $t_\odot$ of the luminosity and radius depend on the initial hydrogen abundance and the mixing-length parameter, α. These are modified by a series of Newton-Raphson iterations until the luminosity and radius agree with $L_\odot$ and $R_\odot$ (the present-day luminosity and radius) to within one part in 10^6. Sufficiently many grid points are required in the temporal and spatial integrations that their relative truncation errors are less than 10^{-6}.

3. Physical assumptions

3.1. Solar age and luminosity

Estimates of the age of the oldest meteorites set a lower bound on the age of the solar system as a whole, and on the age of the sun in particular. Without access to all the meteoritic data, Guenther (1989) recommended a value of 4.49 Gyr. More recent studies suggest the value should be nearer 4.6 Gyr (e.g. Bahcall et al. 1995), and it is this value which is adopted here. At any rate, the correct value for the solar age remains one of the more uncertain ingredients of solar modelling.

The luminosity is also a somewhat uncertain quantity due to the difficulty of calibrating satellite radiometers, and also due to its inherent long-term variability. The value adopted here is the same as that used by Bahcall et al. (1995), namely $3.844 \times 10^{33} \mathrm{erg\,s^{-1}}$.

3.2. Element abundances

The relative abundances of elements in the solar interior are determined by a combination of meteorite analysis and photospheric line strength measurement. The former gives the initial, homogeneous, composition of the primeval solar nebula, while the latter reflects the present-day composition of the outer layers. Apart from the depleted elements Li and Be, the agreement between the two has improved greatly during recent years as improvements have been made in the atomic data which affect photospheric abundance measurements. This enables us to have greater confidence in our knowledge both of the relative abundances of the heavy elements, and also of Z/X, the ratio of heavy-element abundance to hydrogen abundance. Current best estimates are given for these quantities by Grevesse & Noels (1993), and are adopted in the present work; the recommended value for Z/X is 0.0245.

3.3. Energy generation

Thermonuclear energy generation is by the three branches of the proton-proton chain and by the CNO cycle. The energy production per unit mass is computed using a subroutine written by Bahcall (Bahcall & Pinsonneault 1992a, 1992b), with cross sections taken from Bahcall & Pinsonneault (1992a), and energy releases for each reaction taken from Bahcall & Ulrich (1988).

3.4. Equation of state

There are two broad approaches to the problem of finding the thermodynamic properties of a partially-ionized plasma. The chemical-picture approach, of which the Saha equation is an example, is based on the principle of free-energy minimization. The partition function, $\hat{Z}$, of the plasma is assumed to be factorizable into a part corresponding to the internal excitation states of individual particles, and a part corresponding to their translational states. The free energy, $-kT \ln \hat{Z}$, where k is Boltzmann's constant, is then minimized with respect to variations in the occupation numbers which satisfy appropriate stoichiometric constraints. The Saha equation is the simplest realization of this procedure, but suffers from the disadvantage that it predicts unphysical recombination of ions and electrons in the solar centre. There have been several attempts to alleviate this problem. In the CEFF equation of state, Eggleton et al. (1973) introduced an extra term into the free energy which forced complete ionization in the solar centre, although there was no physical justification for this addition. Mihalas et al. (1988) considered an occupation-probability formalism which effectively provided a density-dependent cut-off in the internal part of the partition function. This again predicted almost complete ionization in the solar centre. The Mihalas, Hummer and Däppen (MHD) equation of state was published in the form of tables for a single heavy-element abundance of $Z = 0.02$, and for a heavy-element mixture of carbon, nitrogen, oxygen and iron.

Table 2. Relative heavy-element abundances.

Element	Relative mass fraction	Relative number fraction
C	0.1906614	0.2471362
N	0.0558489	0.0620778
O	0.5429784	0.5283680
Ne	0.2105114	0.1624178

In this study, a new MHD-like equation of state, MHD-E, is calculated using a code written by the author, with energy-level data kindly provided by W. Däppen. Relativistic effects are included in the calculation of the electron free energy (they were not in either OPAL or MHD), which will be seen to have a significant effect on the computed models. The relative heavy-element abundances are set equal to those used in the calculation of the OPAL tables, while the total heavy-element abundance, Z, may be varied, overcoming the limitation of the original MHD tables.

The other approach to the equation of state is known as the physical picture. It does away with the concept of atoms, considering only fundamental particles such as nuclei and electrons. Interactions between particles are taken into account using the techniques of many-body theory. The only realization of these ideas has been carried out by the OPAL group at Livermore, with the publication of preliminary tables in 1994 and subsequently of tables with a finer mesh (Rogers et al. 1996). These tables are computed using the Grevesse (1993) abundances for carbon, nitrogen and oxygen, with the abundances of all the other heavy elements being added to the abundance of neon (see Table 2); they cover $Z = 0.00$, $Z = 0.02$ and $Z = 0.04$. Various comparisons have been made between the OPAL and MHD equations of state (Däppen et al. 1990, Däppen 1992), with the conclusion that they are remarkably similar over the bulk of the solar interior, with OPAL also predicting almost complete ionization at the solar centre; a full explanation for this has yet to be found.

Evolutionary models are computed using both equation of state formalisms. The pressure and other thermodynamic quantities are evaluated as functions of the density, temperature, hydrogen and overall heavy-element mass fractions by means of interpolating tables. Some studies have ignored the variation of the overall heavy-element mass fraction in the calculation of the equation of state, using instead a constant, prescribed value (e.g. Morel et al. 1997). We perform a comparison of models calculated with and without this assumption in order to test its significance. In our best model, we choose only to ignore the variation of the *individual* heavy-element abundances.

Table 3. Comparison of the properties of solar models.

Model	$X_{\rm init}$	α	$X_{\rm c}$	$Y_{\rm surf}$	$Z_{\rm surf}$	$T_{\rm c}$ (10^6K)	$\rho_{\rm c}$ (g cm^{-3})	$\Phi_{^{37}{\rm Cl}}$ (SNU)	$\Phi_{^{71}{\rm Ga}}$ (SNU)	$x_{\rm CZ}$
opal	0.7192	1.9351	0.3618	0.2634	0.0176	15.468	150.79	6.36	122.4	0.726
ydiff	0.7173	2.0983	0.3463	0.2365	0.0183	15.588	154.82	7.22	127.0	0.711
zdiff	0.7115	2.0792	0.3395	0.2422	0.0181	15.671	154.83	7.86	130.4	0.712
zdiffop	0.7116	2.0754	0.3396	0.2421	0.0181	15.670	154.78	7.84	130.4	0.712
mhd	0.7092	2.0383	0.3380	0.2439	0.0181	15.677	154.96	7.93	130.8	0.712
mix	0.7127	2.0707	0.3409	0.2438	0.0181	15.656	154.71	7.73	129.8	0.712
zdiffre	0.7104	2.0683	0.3389	0.2430	0.0181	15.672	154.90	7.87	130.5	0.712
Proffitt (1994)[a]	0.6984	1.711	0.3288	0.7290	0.0196	15.81	155.9	9.02	136.9	0.712
Bahcall & Pinssoneault (1995)[b]	0.7025	2.09	0.3333	0.7351	0.0180	15.84	156.2	9.3	137	0.712
Richard et al. (1996)[c]	0.7012	1.768	0.3328	0.7226	0.0190	15.67	154.53	8.49	132.8	0.716
Christensen-Dalsgaard et al. (1996)[d]	0.7091	1.9905	0.3353	0.7373	0.0181	15.668	154.24	8.2	132	0.712
Morel et al. (1997)[e]	0.7064	1.92	0.3412	0.737	0.0180	15.65	151.2	8.27	130	0.711

[a] CEFF equation of state, age of 4.6 Gyr, $Z/X = 0.0269$.
[b] CEFF equation of state, age of 4.57 Gyr.
[c] MHD equation of state, includes rotation induced mixing.
[d] OPAL equation of state, age of 4.6 Gyr.
[e] OPAL equation of state, age of 4.55 Gyr.

3.5. Opacity

As was the case for the equation of state, the opacity is obtained from interpolating tables. The tables are constructed using the OPAL opacities (Rogers & Iglesias 1992), calculated with the Grevesse (1993) heavy-element mixture, except at low temperatures ($\lesssim 10^4$ K), where the Kurucz (1991) low-temperature opacities are substituted. The interpolation is carried out using a package written by G. Houdek (Houdek & Rogl 1996), which allows a choice between a minimum-norm and a birational-splines algorithm. There is also a freedom of choice in the number of fitting points used in the X and Z interpolations (2,3 or 4). In the first instance the minimum-norm algorithm is used with four fitting points; the effect of other choices on the calibrated hydrogen abundance and mixing-length parameter is investigated in Sect. 4.2.

The heavy-element abundance used to interpolate the opacity tables only includes the abundance changes due to element segregation, since nuclear burning by the CNO cycle has little effect on the opacity (Proffitt 1994). As with the equation of state, the variation of the individual heavy-element abundances is ignored; as suggested by Morel et al. (1997), this may well have a significant effect on the computed models relative to the high precision of p mode frequency data.

4. Results

4.1. Models constructed

The MoSEC code is used to construct a series of calibrated, evolutionary solar models. For all the models, the matching optical depth, $\tau_{\rm b}$, is chosen to be 2, while a global truncation error of better than 10^{-6} is sought. From the considerations of Sect. 2, 1000 radial grid points is sufficient to meet this requirement in the space dimension, while Richardson extrapolation with $Q = 10, 20, 40$ provides sufficient accuracy in time. The models constructed are as follows:

- opal : solar model constructed using the OPAL equation of state with no settling or diffusion of helium or heavy elements.
- ydiff : solar model including the settling and diffusion of helium, and using the OPAL equation of state.
- zdiff : solar model including the settling and diffusion of helium and heavy elements, and using the OPAL equation of state.
- zdiffop : solar model including the settling and diffusion of helium and heavy elements, using the OPAL equation of state without taking into account the variation of the heavy-element abundance.
- mhd : solar model including the settling and diffusion of helium and heavy elements, using the MHD equation of state.
- mix : solar model including the settling and diffusion of helium and heavy elements, using the OPAL equation of state, and including a simple model of turbulent mixing below the base of the convection zone.
- zdiffre : solar model including the settling and diffusion of helium and heavy elements, using the OPAL equation of state, and including the relativistic correction to the electron pressure.

Table 4. The effect on the calibrated hydrogen abundance and mixing-length parameter of the choice of opacity interpolation method and number of interpolation points.

Interpolation method	Number of points	$X_{\rm init}$	α
minimum norm	2	0.718695	1.94696
	3	0.719119	1.94486
	4	0.719232	1.94403
birational splines	4	0.719177	1.94298

Table 5. The effect on the calibrated hydrogen abundance and mixing-length parameter of changing the fineness of the equation of state grid.

EOS grid	$X_{\rm init}$	α
coarse	0.716636	1.890395
fine	0.716632	1.889529

In all cases, the heavy elements are initially chosen to be in the Grevesse & Noels (1993) proportions and iteration is performed to ensure that the final surface heavy-element mass fraction satisfies $Z/X = 0.0245$ (see Sect. 3.2). It would be possible in the case of the models with heavy-element settling and diffusion to iterate the individual heavy-element abundances to ensure that the final surface abundances are in the Grevesse & Noels (1993) proportions, a procedure carried out by Richard et al. (1996). However, bearing in mind that neither the equation of state nor opacity calculation takes into account the variation of individual heavy-element abundances, we do not believe that this procedure would have a significant effect, and therefore do not include it at present.

Various properties of the computed models are listed in Table 3 and compared with the properties of a selection of other recent solar model calculations which include settling and diffusion of helium and heavy elements. $X_{\rm c}$, $T_{\rm c}$ and $\rho_{\rm c}$ denote the central hydrogen mass fraction, central temperature and central density respectively. $X_{\rm init}$ denotes the initial (uniform) hydrogen mass fraction, $Y_{\rm surf}$ denotes the final surface helium mass fraction, $Z_{\rm surf}$ denotes the final surface heavy-element mass fraction, while $x_{\rm CZ}$ denotes the fractional radius of the base of the convection zone. $\Phi_{^{37}\rm Cl}$ and $\Phi_{^{71}\rm Ga}$ represent the predicted neutrino capture rates for ^{37}Cl and ^{71}Ga detectors, given in solar neutrino units (1 SNU = 10^{-36} capture atom^{-1} s^{-1}).

4.2. *Opacity and equation of state interpolation*

A series of models is constructed using the two different opacity interpolation methods (minimum norm, and birational splines) and various different numbers of fitting points (2,3 and 4); all other aspects of the physics (OPAL equation of state, no settling or diffusion) are kept constant. The calibrated hydrogen abundances and mixing-length parameters for these models are listed in Table 4. The third model listed corresponds to the "opal" model in table 3.

As can be seen from this table, there is a reasonably good agreement between models constructed using the two different interpolation algorithms with four interpolation points. The agreement is better for the initial hydrogen abundance than for the mixing-length parameter, which is as expected given that the latter is more sensitive to the opacity. The three models constructed with the birational-spline algorithm show, as expected, that as the number of interpolation points is reduced, the calibrated hydrogen abundance and mixing-length parameter exhibit increasingly large errors.

The effect of changing the fineness of the grid used in the equation of state tables is shown in Table 5. Both the models listed in this table are constructed without helium settling or diffusion, using the MHD equation of state; the first is constructed using equation of state tables on the same grid as the OPAL equation of state, while the second is a similar model constructed using MHD equation of state tables with a grid twice as fine. The differences between the two models in this case are smaller (much smaller in the case of the hydrogen abundance) than the differences described above between models calculated using two different opacity interpolation schemes. The errors introduced by interpolation (especially in the calibrated hydrogen abundance) are therefore dominated by the those arising from the opacity interpolation. The original choice of grid for the MHD equation of state tables (corresponding to that used in the OPAL tables) is therefore sufficiently fine.

4.3. *Microscopic diffusion*

It is well known that models without settling and diffusion of helium do not very well reproduce the seismically determined surface helium abundance and convection-zone depth of the sun (e.g. Christensen-Dalsgaard et al. 1993, Proffitt 1994), having surface helium abundances too high, and convection-zone depths too low. In this study, including settling and diffusion of helium decreases $Y_{\rm surf}$ from 0.2634, in the case of the "opal" model, to 0.2365, in the case of the "ydiff" model, and decreases $x_{\rm CZ}$ from 0.726 to 0.711. These are similar findings to those of Christensen-Dalsgaard et al. (1993). Comparison may be made with the seismically determined values of ~ 0.25 (Däppen et al. 1988, Vorontsov et al. 1991, Basu & Antia 1995, Dziembowski et al. 1994) for $Y_{\rm surf}$, and 0.713 ± 0.003 (Christensen-Dalsgaard et al. 1991b) for $x_{\rm CZ}$.

In addition to improving the agreement in convection-zone depth and surface helium abundance, helium settling and diffusion dramatically improve the agreement in sound-speed with the sun. This is shown in Fig. 3, where the dashed line represents the relative difference in squared sound speed, $\delta c^2/c^2$, between the "opal" model and the sun, and the dotted line represents the same quantity for the "ydiff" model. This improvement is principally due to the increased convection-zone depth, but also

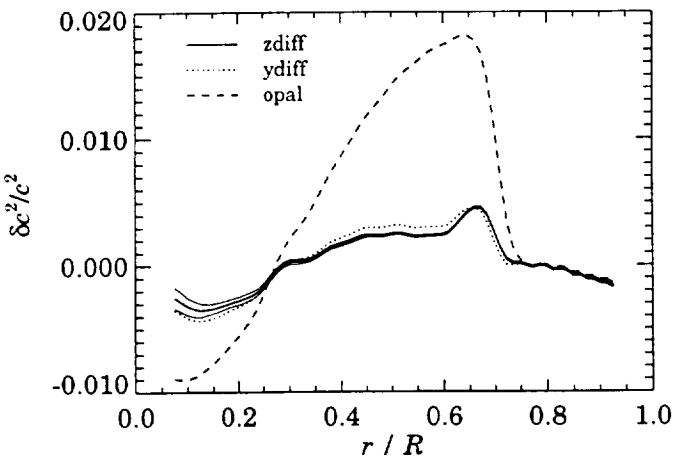

Fig. 3. The difference in squared sound speed between the models zdiff, ydiff and opal and the sun, plotted as a function of fractional solar radius, constructed from an inversion of 2 months of MDI p mode frequency data with model S of Christensen-Dals gaard et al. (1996) as reference. The thin solid lines show the standard errors in the sound-speed inversion.

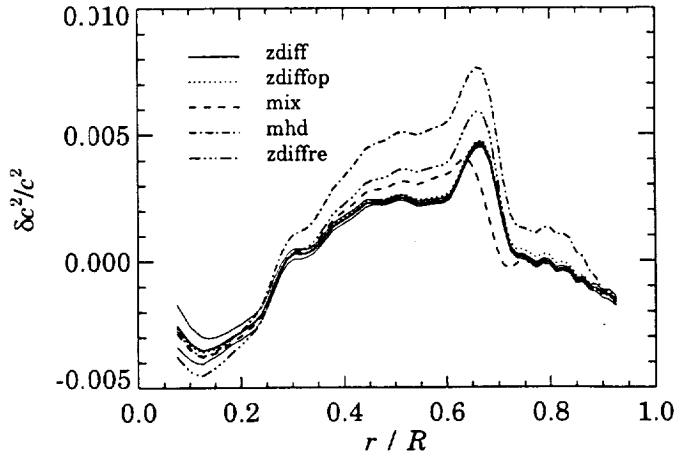

Fig. 4. The relative difference in squared sound speed between the models zdiff, zdiffop, mix, mhd and zdiffre and the sun, constructed in the same way as in Fig. 3. The thin solid lines represent the standard errors in the sound-speed inversion.

partly due to the reduced mean molecular weight just below the base of the convection zone. There are still significant features just below the base of the convection zone, where the sound speed is too low in the model, and near the centre, where the sound speed is too high in the model.

Heavy-element settling and diffusion have been included in many of the recent solar model calculations, including all the models listed in the lower half of Table 3. These processes are included in model "zdiff", increasing $Y_{\rm surf}$ by 0.0057 and reducing $x_{\rm CZ}$ by 0.001, in very close agreement with the results of Proffitt (1994). The corresponding form of $\delta c^2/c^2$, shown by the thick solid line in Fig. 3, is very similar to that found for the "ydiff" model, with a maximum difference of about 0.05% in sound speed between the two models at around $r/R_\odot = 0.5$ (which is, nevertheless, significant compared to the errors in the inversion, shown by the thin solid lines). Consequently, unlike helium, heavy-element settling and diffusion do not significantly improve the agreement in sound speed between solar models and the sun.

The flux of neutrinos arising from the decay of ^{8}B is strongly affected by the inclusion in the evolution calculation of the diffusion and settling of helium and heavy-elements. Gravitational settling leads to an increase in mean molecular weight at the centre, and a consequent increase in the central temperature. This leads to an increase in the flux of ^{8}B neutrinos (since the latter goes roughly like T^{16} at the solar centre). Bahcall & Pinsonneault (1992b) found that helium settling alone brought about an increase of about 12% in the flux measured by the chlorine neutrino capture experiments; Proffitt (1994) found an increase in this flux of about 13.6%, the discrepancy being due to the different formulations of the diffusion equations for helium. In this study, we find that the ^{37}Cl flux goes from 6.12 SNU to 6.95 SNU, an increase of about 14%; this is very close to the value obtained by Proffitt (1994).

We find that helium and heavy-element settling combined produce an increase in the ^{37}Cl flux of about 24%. There is considerable variation in the corresponding increase found by other authors, varying from 15% (Richard et al. 1996) to 32% (Bahcall & Pinsonneault 1995); Turck-Chièze & Brun (1997) find an increase of 26%, closest to our result. The reasons for these wide discrepancies are not yet clear. In terms of the actual ^{37}Cl flux prediction, all the models listed in Table 3 predict a somewhat higher ^{37}Cl flux than the model "zdiff", although the calculations of Turck-Chièze & Brun (1997) predict a lower ^{37}Cl flux of 7.2 SNU.

4.4. The equation of state

The model "zdiffop" is constructed only taking into account the variation of the overall heavy-element abundance, Z, in the interpolation of the opacity tables. This is a similar assumption to that made by Morel et al. (1997). The relative difference in squared sound speed between this model and the sun is shown by the dotted line in Fig. 4, and compared with the same quantity for four other models, "zdiff" (solid line), "mhd" (dot-dashed line), "mix" (dashed line) and "zdiffre" (dot-dot-dot-dashed line). The relative differences in squared sound speed between the models "zdiffop", "mix", "mhd" and "zdiffre" and the model "zdiff" are plotted in Fig. 5 using the same line styles. As can be seen, the difference in $\delta c^2/c^2$ between "zdiffop" and "zdiff" is almost within the standard errors in the inversion (shown by the thin solid lines), and the neglect of the variation of the overall heavy-element abundance in the calculation of the equation of state is therefore valid. It therefore seems that, contrary to the claims of Morel et al. (1997), equation of state data taking into account detailed changes in the heavy-element mixture are unnecessary.

Comparison is made between the OPAL and the MHD-E equations of state using the "mhd" model, which differs from the "zdiff" model only in using the MHD-E instead of the OPAL equation of state. Early comparisons of the OPAL and MHD

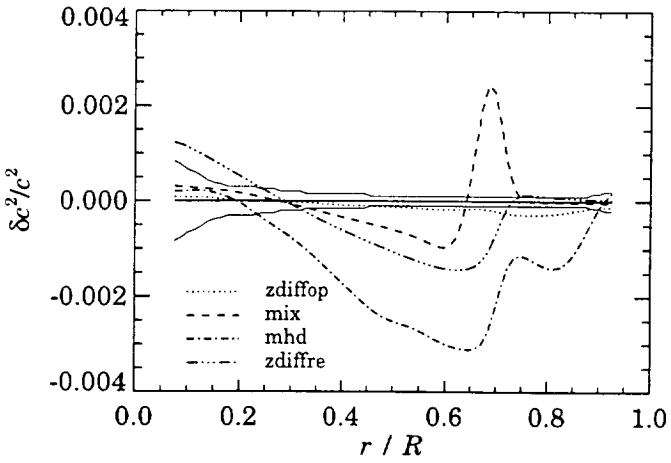

Fig. 5. The relative difference in squared sound speed between the models zdiffop, mix, mhd and zdiffre and the model zdiff. The thin solid lines represent the standard errors in the sound-speed inversion.

equations of state (Däppen et al. 1990, Däppen 1992) found very close agreement over most of the solar interior. More recently, Guenther et al. (1996) computed models using both equation of state formalisms, finding very close agreement both in global properties and in local physical quantities, while Rogers et al. (1996) found slight differences in the location of the hydrogen and helium ionization zones leading to a so-called "pressure spike" in the MHD equation of state at temperatures of $\sim 50\,000$ K.

In the present calculation, the two models "mhd" and "zdiff" do not agree as closely as those of Guenther et al. (1996), with larger differences in initial hydrogen abundance, mixing-length parameter, and also in the sound speed. However, better agreement is found when the "mhd" model is compared to the "zdiffre" model, which uses the OPAL equation of state but includes a correction for relativistic effects. This shows that the inclusion of the relativistic correction in the new MHD-E equation of state accounts for much of the difference found between the "mhd" and "zdiff" models. The relativistic correction has the effect of increasing the electron pressure at the centre, thus reducing the hydrogen abundance there in the calibrated model. This has a significant effect on the sound speed throughout the radiative interior, reducing it by a maximum of about 0.1% near the base of the convection zone.

4.5. Sub convection-zone mixing

A simple model of the sub convection-zone mixing associated with the solar tachocline (Spiegel & Zahn 1992, Elliott 1997) is included in the model "mix". Instead of assuming complete mixing to the base of the convection zone, as in the standard solar model prescription, the region of mixing is assumed to extend a distance of $0.02R_\odot$ below the base of the convection zone: this value is somewhat lower than the thickness of the tachocline as inferred from rotation-rate inversions (Kosovichev 1996). The effect of the extra mixing is to redistribute gravitationally settled helium back into the convection zone, thereby reducing the mean molecular weight just below the base of the convection zone. This, in turn, increases the sound speed in that region as is shown by the dashed line in Fig. 5. Deeper down, the recalibration of the model reverses the situation, causing the sound speed to be lower in "mix" than in "zdiff". The overall effect of the extra mixing is to improve slightly the agreement in sound speed with the sun: the sound speed increase in the "mix" model relative to the "zdiff" model would need to be displaced downward to account fully for the hump in $\delta c^2/c^2$ just below the base of the convection zone.

5. Conclusion

The new solar evolution code described in this paper has been shown to produce results broadly consistent with previous calculations, as well as having well-controlled truncation errors both in space and time. The effects of using interpolating tables for the opacity and equation of state have been quantified, with the conclusion that at present the interpolation of the OPAL opacity tables sets the limit on errors in the calibrated hydrogen abundance and mixing-length parameters.

The effect of including helium diffusion and settling in the evolution calculation is very similar to that found by previous authors. There is a significant increase in the predicted neutrino flux for the chlorine experiments (14%), and a somewhat smaller increase (3.8%) for the gallium experiments. When heavy-element diffusion is also included, the corresponding increases relative to the non-diffusive models are 23% and 6.5%, both similar to the values found by Turck-Chièze & Brun (1997). The actual value of the predicted count rate for the chlorine experiment, 7.86 SNU, is somewhat smaller than that reported by most other authors, but larger than the 7.2 SNU reported by Turck-Chièze & Brun. These differences point to the need for further investigation.

The inclusion of the variation of the overall heavy-element mass fraction in the calculation of the equation of state has been shown to have an almost negligible effect on the sound speed on the computed model, rendering the effect of the variation of *individual* heavy-element abundances in the equation of state calculation undetectable at the current precision of structure inversions. This is, however, not the case in the calculation of the opacity, and opacity data taking into account detailed changes in composition are necessary.

A comparison is provided here between models constructed using the OPAL and MHD-E equations of state. The agreement is not as good as that reported in previous comparisons between OPAL and MHD, principally due to inclusion of the relativistic correction to the electron pressure in the newly-calculated MHD-E equation of state. The significant effect that this correction has on the sound speed of calibrated models should perhaps prompt efforts to include it consistently in future equation of state calculations.

A simple model of the sub convection-zone mixing associated with the solar tachocline has been shown to improve the agreement in sound speed with the sun just below the base of the

convection zone. Further study is required to understand fully the sound speed enhancement found in this region of the sun.

In spite of improvements in solar evolution calculations, it is as well to point out that there are still considerable unknowns in many of the physical assumptions (Gough & Toomre 1991). The high accuracy of the calculation presented here facilitates detailed comparison with models by other authors, but belies some of the inherent uncertainties. Perhaps most serious is the assumption of uniform chemical composition at zero age, which is contingent on the sun having passed through a fully-convective Hayashi phase of evolution. Calculations by Larson (1969) have suggested that this may not have occurred. Another significant failing of the standard solar model is its neglect of large-scale macroscopic motions (aside from convection). It is known that such motions must occur in any rotating star, which could have important repercussions for its evolution by redistributing both material and angular momentum. Mass loss and accretion are known to be important processes in stellar evolution but are again entirely neglected in the standard solar model prescription. The modular nature of MoSEC should permit refinements of the physical assumptions to be easily incorporated, allowing the code to keep pace with our improving understanding of solar evolution.

Acknowledgements. We thank J. Toomre for useful comments on improving the presentation of the paper, and W. Däppen for providing energy-level tables for use in calculating the MHD equation of state. We also want to thank the referee of this paper, S. Turck-Chièze, who suggested other useful improvements. This work is supported in part by the National Aeronautics and Space Administration through grants NAG5-2256 and NAG5-3077.

References

Anders E., Grevesse N., 1989, Geochim. Cosmochim. Acta, 53, 197
Ando H., Osaki Y., 1975, PASJ, 27, 581
Bahcall J.N., 1989, Neutrino Astrophysics. Cambridge Univ. Press, Cambridge
Bahcall J.N., Loeb A., 1990, ApJ, 360, 267
Bahcall J.N., Pinsonneault M.H., 1992a, Rev. Mod. Phys., 64, 885
Bahcall J.N., Pinsonneault M.H., 1992b, ApJ, 395, L119
Bahcall J.N., Pinsonneault M.H., 1995, Rev. Mod. Phys., 67, 781
Bahcall J.N., Ulrich R.K., 1988, Rev. Mod. Phys., 60, 297
Basu S., Antia H.M., 1995, MNRAS, 276, 1402
Berthomieu G., Provost J., Morel P., Lebreton Y., 1993, A&A, 268, 775
Burgers J.M., 1969, Flow Equations for Composite Gases. Academic Press, New York
Cash J.R., Moore D.R., 1980, B.I.T., 20, 44
Christensen-Dalsgaard J., 1991a, in: Gough D., Toomre J. (eds.) Challenges to Theories of the Structure of Moderate-Mass Stars, Lecture Notes in Physics, Vol. 388. Springer, Heidelberg, p. 11
Christensen-Dalsgaard J., Gough D.O., Thompson M.J., 1991b, ApJ, 378, 413
Christensen-Dalsgaard J., Proffitt C.R., Thompson M.J., 1993, ApJ, 403, L75
Christensen-Dalsgaard J., The GONG Project Team, 1996, Sci, 272, 1286
Däppen W., 1992, Rev. Mex. Astron. Astrofis., 23, 141
Däppen W., Gough D.O., Thompson M.J., 1988, in: Domingo V., Rolfe E.J (eds.) ESA SP-286, Proc. Symp. Seismology of the Sun and Sun-Like Stars. ESA, Noordwijk, p. 505
Däppen W., Lebreton Y., Rogers F.J., 1990, Solar Phys., 128, 35
Dziembowski W.A., Goode P.R., Pamyatnykh A.A., Sienkiewicz R., 1994, ApJ, 432, 417
Elliott J.R., 1997, A&A, 327, 1222
Eggleton P.P., Faulkner J., Flannery B.P., 1973, A&A, 23, 325
Gough D.O., Toomre J., 1991, ARA&A, 29, 627
Grevesse N., Noels A., 1993, in: Prantzos N., Vangioni-Flam E., Cassé M. (eds.) Origin and Evolution of the Elements. Cambridge Univ. Press, Cambridge, p. 15
Guenther D.B., 1989, ApJ, 339, 1156
Guenther D.B., Kim Y.-C., Demarque P., 1996, ApJ, 463, 382
Harvey J.W., The GONG Project Team, 1996, Sci, 272, 1284
Houdek G., Rogl J., 1996, Bull. Astr. Soc. India, 24, 317
Iglesias C.A., Rogers F.J., 1991, ApJ, 371, 408
Kosovichev, A.G. 1996, ApJ, 469, L61
Kosovichev A.G., The MDI Project Team, 1997, Solar Phys., 170, 1
Kurucz R.L., 1991, in: Crivellary L., Hubeny I., Hummer D.G. (eds.) Stellar Atmospheres: Beyond Classical Models. Kluwer, Dordrecht, p. 440
Larson R.B., 1969, MNRAS, 145, 271
Michaud G., Proffitt C.R., 1993, in: Weiss W.W., Baglin A. (eds.) IAU Coll. 137, Inside the Stars. Astronomical Society of the Pacific, San Francisco, p. 246
Mihalas D., Däppen W., Hummer D.G., 1988, ApJ, 331, 815
Morel P., Provost J., Berthomieu G., 1990, Solar Phys., 128, 7
Morel P., van't Veer C., Provost J., Berthomieu G., Castelli F., Cayrel R., Goupil M.J., Lebreton Y., 1994, A&A, 286, 91
Morel P., Provost J., Berthomieu G., 1997, A&A, 327, 349
Proffitt C.R., 1994, ApJ, 425, 849
Richard O., Vauclair S., Charbonnel C., Dziembowski, W.A., 1996, A&A, 312, 1000
Rogers F.J., Iglesias C.A., 1992, ApJS, 79, 507
Rogers F.J., Swenson F.J., Iglesias C.A., 1996, ApJ, 456, 902
Spiegel E.A., Zahn, J.-P. 1992, A&A, 265, 106
Turck-Chièze S., Lopes I., 1993, ApJ, 408, 347
Turck-Chièze S., Brun, A.S., 1997, preprint
Vorontsov S.V., Baturin V.A., Pamyatnykh A.A., 1991, Nat, 349, 49
Willson R.C., Hudson H.S., Frölich C., Brusa R.W., 1986, Sci, 234, 1114